A coarse grain model of microtubules

Shuo Feng, and Haiyi Liang[a)]

CAS Key Laboratory of Mechanical Behavior and Design of Materials, Department of Modern Mechanics,
University of Science and Technology of China, Hefei, Anhui 230027, China

Abstract This paper proposes a 3-dimensional coarse grain model of microtubules and treats the tubulin monomer as a sphere of multiple patches, with parameters chosen to yield experimental values of bending and stretching stiffness. The model has demonstrated the ability to produce the bistability of tubulin sheets, elastic deformation near the tip, and cracking and peeling of protofilaments. This model is expected to take into account the structural and mechanical aspects underlying the physical mechanism of polymerization/depolymerization and dynamic instability of microtubules. © 2012 *The Chinese Society of Theoretical and Applied Mechanics.* [doi:10.1063/2.1201406]

Keywords microtubule, patchy sphere, spontaneous curvature, bistable, dynamic instability

Microtubules (MTs) are polar linear polymers of protein tubulin heterodimers found ubiquitously in eukaryotes. The MTs together with actin and intermediate filaments form cytoskeletal networks, which determine the mechanics of cells, and perform various essential biological functions including chromosome segregation, motor proteins transportation and cell locomotion.[1] The MT usually consists of 13 protofilaments (PFs), assembled in parallel by lateral interactions into hollow cylindrical shell of approximately 25 nm in the outer diameter and 5 nm in the thickness. Such tubular arrangement makes MT the stiffest element compared to other two cytoskeletal filaments. Accordingly, the persistence length l_p ($l_\mathrm{p} = \kappa/k_\mathrm{B}T$, where κ is the bending stiffness) of MTs ranges from hundreds to thousands of micrometers[2] in comparison with the typical size of an eukaryotic cell ranging from 10 to 100 micrometers. Instead of being static, the length of MTs switches repeatedly and stochastically between slow growing and rapid shrinking phases both *in vivo* and *in vitro*, a dramatic nonequilibrium phenomenon called dynamic instability[3] allows for force generation and remodeling of cytoskeleton spatial organization during mitosis or exploration of the surrounding environment.

The MT dynamic instability roots in the molecular details of tubulin dimers during polymerization and depolymerization. The molecular structure of α and β monomers are highly homologous. Each tubulin monomer resembles an ellipsoid of dimension 4.6 nm × 4.0 nm × 6.5 nm, formed by a core of two β sheets surrounded by α helices and identified functionally into three binding domains.[4] Either of the monomers binds one guanosine triphosphate (GTP) molecular at the N-terminal nucleotide-binding domain. A non-exchangeable GTP at the N-site in α-tubulin is fully buried in the intradimer interface, while the GTP bound at the E-site on the free surface of β-tubulin is exchangeable and hydrolyzable.[1] When tubulin dimers polymerize head-to-tail into PFs, the partially exposed β-tubulin GTP is then buried non-exchangeably in the newly formed interdimer interface and shortly hydrolyzes to guanosine diphosphate (GDP) catalyzed by α-tubulin residues.

It is now accepted that the nucleotide state plays a central role in connecting monomers. The longitudinal intra- and inter-dimer contacts are distinct despite their similarity in electron density map. The GTP monomer-monomer interface is significantly strong with less bending while GDP dimer-dimer interface is much flexible and prone to large kinking, due to residues difference and local conformation change.[5] A free-standing GDP-bound PF will naturally bend, but it is forced to straighten by the constraints from neighboring PFs in MT lattice. The chemical energy from GTP hydrolysis is thus stored in the apparently straight MT in the form of elastic energy, which promotes a transition to shrinkage, i.e. catastrophe. The lateral aggregation of PFs into tubule results in large part from the interactions of M-loop and helix H3 between adjacent monomers. This lateral contact is of weak electrostatic effects in contrast to the hydrophobic and polar nature of longitudinal contacts.[6] The highly stressed plus-end of MTs tends to disassemble especially when the lateral contact is weakened by the conformation change in helix H3 associated with GTP hydrolysis. It is proposed that a layer of GTP cap or an equivalent structural cap of strong lateral contact is required to stabilize MTs, otherwise catastrophe is triggered.

Despite the substantial experimental understandings in the molecular details of tubulin, the physical mechanism underlying dynamic instability remains unclear. Various theoretical and computational models have quantified phenomenologically the stochastic growth and shrinkage in kinetic view by assuming the rate of addition and hydrolysis of tubulin.[7,8] However, the mechanical and structural features are the crucial ingredients of dynamic instability. Several coarse-grained simulations considering elasticity explicitly have been devoted to understand mechanical deformation near the cap,[9] force generation of shrinking MTs,[10] length dependence of persistence length,[11] and 3-dimensional structures of sheet-like/blunt tip

---

a)Corresponding author. Email: hyliang@ustc.edu.cn.

and their consequence on catastrophe.[12] An important experimental observation that tubulins first aggregate into intermediate sheets then turn over to closed tubes, is igonred by most computational and theoretical models, which indicates the existence of bistability in MTs.[5,13,14,16] The bistability feature is not surprising since GDP PFs peel outward and at the same time MTs favor lateral curving.

In this study, we propose a 3-dimensional coarse-grain model of MTs, aiming at capturing the crucial role of bistability as well as the structural and mechanical aspects. The α or β tubulin monomer is modeled as a sphere, decorated with 4 orientation-dependent patchy points on the surface (Fig. 1(a)). The adhesion between patches on adjacent spheres can introduce naturally spontaneous curvatures in tubulin aggregation. Polar disk was used in self-assembly of supermolecular[15] and here the idea is extended nontrivially to sphere of multiple polarities. The non-covalent interaction between patchy monomer i and j is described as modified Morse potential (Fig. 1(a))

$$V(r_{ij}) = \epsilon\{[1 - e^{-a(r_{ij}-r_0)}]^2 - 1\}e^{-b(\theta_i^2+\theta_j^2)}, \quad (1)$$

where r_{ij} and r_0 are the current and the rest center-to-center distances respectively, θ_i and θ_j are the relative angles, a and b are the paraments related to bending and stretching stiffness between monomers, and ϵ is the adhesion strength. The standard Morse potential part maintains an equilibrium distance between monomers. The exponential term enforces an orientation requirement that two patches have to eqnarray along the center-to-center line, otherwise the interaction between the two patches decays quickly (Fig. 1(a)). By tuning relative position of patch points, it is possible to generate a bistable MT with spontaneous curvatures of longitudinal outwards and lateral inwards. In addition, this simple model does not require permanent connection among monomers and therefore facilitates simulation of assembly/disassembly based on discrete tubulins.

From Eq. (1) one can calculate important mechanical properties of bending and stretching stiffness, longitudinally and laterally, where parameter a determines the stretching stiffness and parameter b for the bending stiffness. In a straight GTP PF, the rest distance between neighboring dimer-center is $L = 2r_0$. With infinitesimal axial strain δ, one can write down the stretching energy per dimer as

$$U_{\rm s} = (1 - e^{-a\delta L})^2\epsilon - \epsilon \simeq (a\delta L)^2\epsilon. \quad (2)$$

In its continuum analogue of an elastic rod, the stretching energy can be expressed alternatively as

$$U_{\rm s} = \frac{1}{2}S\delta^2 L, \quad (3)$$

where $S = EA$ is the stretching stiffness. By equating the two expressions above, we get the stretching stiffness of a PF

$$S = 2a^2 L\epsilon. \quad (4)$$
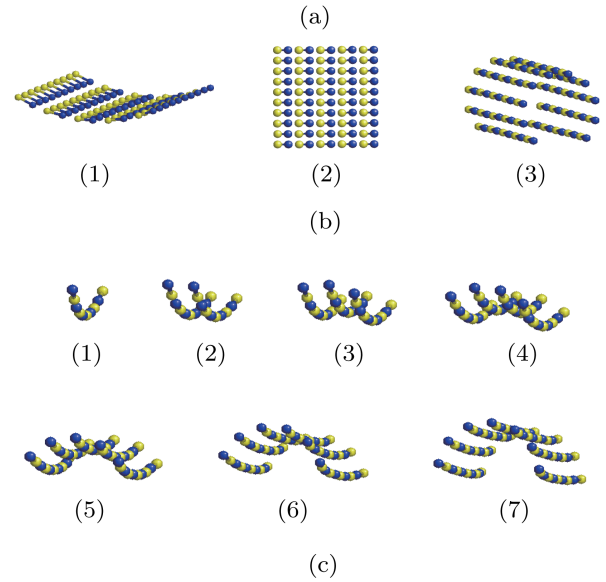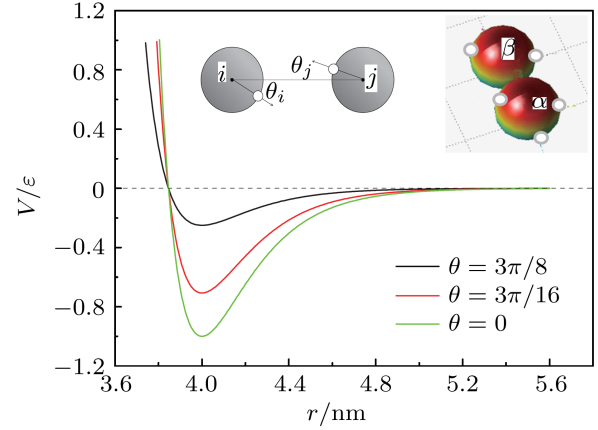
Fig. 1.   (a) The interaction between two patchy monomers. The white dot on the grey sphere is the patchy point. The θ_i and θ_j are the angles between the center-to-patch line and the center-to-center line. When $\theta_i = \theta_j = 0$, the two patchy points eqnarray. Two spheres form a dimer with 6 patchy points (inset). (b) Effect of unidirectional spontaneous curvature on a flat tubulin sheet(middle): the sheet curves upwards with the longitudinal spontaneous curvature and downwards with the lateral spontaneous curvature. The α-tubulin is in yellow and β-tubulin is in blue. (c) With bidirectional longitudinal and lateral natural curvature, increasing the number of PFs causes a turn-over from longitudinal curving to lateral curving. The data of spontaneous curvature are taken from the work by Nogales et al.[17,18]

Similarly, we can obtain the equivalent bending stiffness from the orientation-dependent term in Eq. (1). Assuming a weakly bent PF with relative angles $\theta_i = -\theta_j = \theta \sim o(1)$, the curvature $\kappa \simeq 2\theta/L$ and the discrete form of bending energy per dimer, we have

$$U_{\rm b} = -\epsilon e^{-bL^2\kappa^2/2} + \epsilon \simeq \frac{1}{2}b\kappa^2 L^2\epsilon. \quad (5)$$

The continuum description of bending energy of an elas-

Table 1.   This table lists the longitudinal Young's modulus E, bending rigidity EI, shear modulus G and the outer radius R_o and inner radius R_i of MTs.

	Tubulin Source	E/GPa	R_o&R_i/nm	$EI/(10^{-24}\mathrm{Nm}^2)$	G/Pa
Gittes[19]		1.2	14.18 11.48	21.5±0.8	
Mickey[20]	Bovine	1.4	14.18 11.48	Pure: 62±9 Tao: $34 \pm 3(37°\mathrm{C})$ $21 \pm 1(25°\mathrm{C})$ Taxol: 32±2 Cap: 26±2	
Felgner[21]	Porcine			Pure: 2.9−5.1 Taxol: 0.7−2.0 MAPs: 13−21	
Tolomeo[22]	Mammalian	2	15 8.5	70	10^3
Kis[23]		>0.1	12.5 7.5		$(1.4 \pm 0.4) \times 10^6$
de Pablo[24]	Porcine	0.8			
Tuszynski[25]		Long.: 1.32 Lat.: 0.004	12.5 7.5		$53.0 - 50 \times 10^6$
Pampaloni[2]	Porcine	1.51±0.19	12.5 7.5		
Zeiger[26]		Long.: 1.25(α) 1.34(β) Lat.: 0.8356(α) 0.6584(β)			
Sept[27]		Apo: 2.2 Taxol: 0.38	12 8	28.8 14.6	47×10^6 48×10^6
Deriu[28]		−1		4 − 9	50×10^6

tic rod is

$$U_{\mathrm{b}} = \frac{1}{2} B \kappa^2 L. \tag{6}$$

Again by equating the two expressions above, we get the bending stiffness of a PF

$$B = bL\epsilon. \tag{7}$$

The relations (4) and (7) along with the interaction potential (1) allow us to determine the three parameters a, b, and ϵ by using the available data of cohesive energy, stretching stiffness S and bending stiffness B from either experimental measurements or full atom molecular dynamics simulations as summarized in Table 1. We see wild fluctuation that $(0.38 - 2.2)$ GPa for longitudinal Young's modulus, $(0.7 - 71) \times 10^{-24}$ Nm^2 for bending stiffness, and $53.0 - 50 \times 10^6$ Pa for shear modulus. The information about lateral stretching and bending is rare in the literature, perhaps they are regarded as trivial in comparison with the important longitudinal properties. It is then left to us to determine reasonable values of longitudinal/lateral stretching and bending stiffness. Thanks to the longitudinal and lateral adhesion energy of $18.5k_{\mathrm{B}}T$ and $3.2k_{\mathrm{B}}T$, respectively,[29] assuming the radius of a monomer 2 nm, we find $a_{\mathrm{Long}} = 4.5$ nm^{-1} and $b_{\mathrm{Long}} = 72$, corresponding to longitudinal Young's modulus $E_{\mathrm{Long}} = 1.97$ GPa and bending stiffness $B_{\mathrm{Long}} = 2.21 \times 10^{-26}$ Nm^2; respectively for lateral interactions, we choose $a_{\mathrm{Lat}} = 4.5$ nm^{-1} and $b_{\mathrm{Lat}} = 6$ so that $E_{\mathrm{Lat}} = 178$ MPa and $B_{\mathrm{Lat}} = 3.17 \times 10^{-28}$ Nm^2. These parameters are determined with certain arbitrariness, but still comply with the fact that the interactions are strong longitudinally and weak laterally, following the experimental understandings of interactions between tubulin molecular.[1,4,5] Dynamic instability is found to have an inherent property regardless of complications from various effectors like ions, MAPs, and

drugs, indicating the insensitiveness of the patchy model to "exact" parameters if the critical underlying mechanism is captured.

To validate our model, several simulations have been carried out via Monte-Carlo method[30] to study the bistability of tubulin sheets, elastic deformation in the vicinity of MT tip, and peeling of PFs during depolymerization. During the simulations, two spheres are permanently linked mimicking a stable tubulin dimer by fixing the center-to-center distance (inset in Fig. 1(a)). Figure 1(b) shows that a flat tubulin sheet bends upwards with longitudinal spontaneous curvature, or downwards with lateral spontaneous curvature. When the two spontaneous curvatures apply simultaneously, a tubulin sheet changes gradually from bending upwards to downwards as the number of PF increases (Fig. 1(c)), showing the typical characteristic of bistability.

Figure 2(a) and 2(b) plot the displacement of the MT near the tip ($x = 0$) driven by the longitudinal spontaneous curvature κ_0, showing an oscillation of exponential decay. We assume that the deformation is small $w \sim t$, where t is the thickness of the tube. The bending energy is $U_{\mathrm{b}} \sim Bl_{\mathrm{p}}D\kappa^2$, where B is the bending stiffness of PF, $D = 2\pi R$ is the circumferential length.[31] The released stretching energy associated with the circumferential strain w/R is $U_{s2} \sim S_2 Dl_{\mathrm{p}}w^2/R^2$, where S_2 is the circumferential stretching stiffness. Noticing that the two energies should be of the same order $U_{\mathrm{b}} \sim U_{s2}$, we get $w \sim Rt\kappa$. This linear dependence of w on κ is consistent with our simulation result (inset in Fig. 2(a)). To determine persistence l_{p}, we need to consider another stretching energy associated with longitudinal strain release w^2/l_{p}^2, that is $U_{s1} \sim S_1 Dl_{\mathrm{p}}(w^2/l_{\mathrm{p}}^2)^2$. Minimizing the sum of $U_{s1} + U_{s2}$, we see that $l_{\mathrm{p}} \sim (Rw)^{1/2} \sim (Rt)^{1/2}$, noticing $w \sim t$ in our small displacement assumption. Figure 2(c) demon-

(a)

(b)

(c)
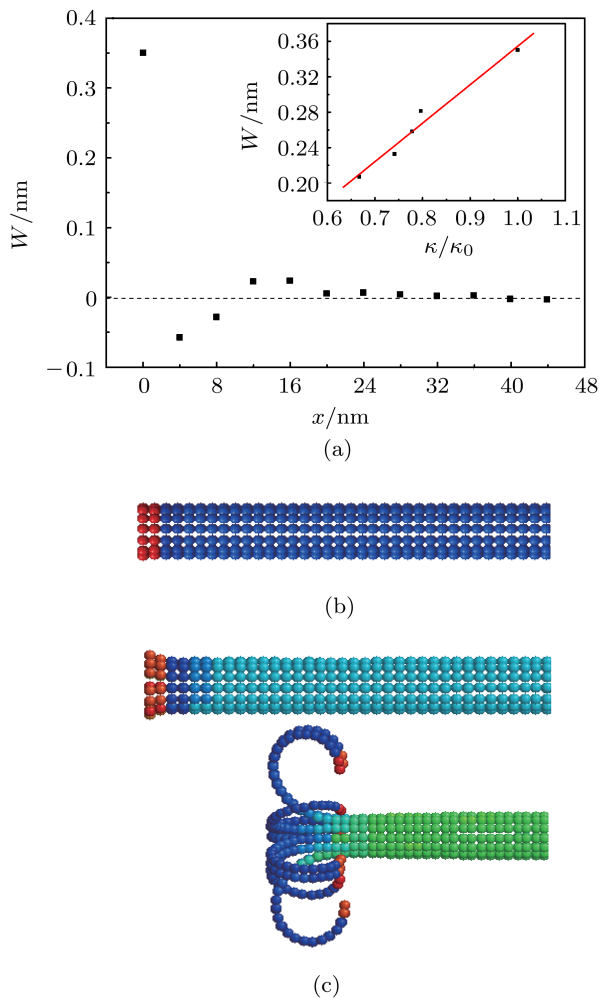
Fig. 2.   (a) The normal deflection w varies with distance x from the free tip. The inset shows a linear relationship between w and the spontaneous curvature κ, as rescaled by the maximum κ_0. (b) The MT constructed in simulation, the left tip is free and the right side is fixed. The elastic energy of tubulin dimers is shown in color, blue for lower energy and red for higher energy. (c) The onset of cracking and peeling of MTs. When the spontaneous curvature is larger than a critical value, MT start to crack and PF peels off.

strates the peeling process of PFs from the tip when the spontaneous curvature reaches a critical value. The radius of the longitudinal curvature of PF is 20 nm, and the radius of the lateral curvature of PF is 12.5 nm. It is interesting to note that once the tip starts to crack, the dimers behind the cracked area have the least elastic energy.

In summary, we proposed a 3-dimensional patchy sphere model of MTs with multiple polarities. The parameters in the monomer-monomer interaction have been reasonably determined, whose uncertainties can be alleviated with better experimental or atomistic simu-

lation values. We validate the patchy model via Monte-Carlo simulations including the demonstration of bistability of tubulin sheets. This model is expected to be able to study structural, mechanical, as well as kinetic aspects underlying the physical mechanism during polymerization/depolymerization of MTs.

1. E. Noglales, Annu. Rev. Biochem. **69**, 277 (2000).
2. F. Pampaloni, G. Lattanzi, and A. Jona, et al, PNAS **27**, 10248 (2006).
3. T. Mitchison, and M. Kirschner, Nature **312**, 237 (1984).
4. E. Nogales, S. G. Wolf, and K. H. Downing, Nature **391**, 199 (1998).
5. H. W. Wang, and E. Noglales, Nature **435**, 911 (2005).
6. E. Noglales, M. Whittaker, and R. A. Milligan, et al, Cell **96**, 79 (1999).
7. B. A. H. Dogterom, and S. Leibler, Phys. Rev. Lett. **70**, 1347 (1993).
8. L. Brun, B. Rupp, and J. J. Ward, et al, Proc. Natl. Acad. Sci. U. S. A. **50**, 21173 (2009).
9. I. M. Janosi, D. Chretien, and H. Flyvbjerg, Eur. Biophys. J. **27**, 501 (1998).
10. M. I. Molodtsov, E. L. Grishchuk, and A. K. Efremov, et al, Proc. Natl. Acad. Sci. U. S. A. **12**, 4353 (2005).
11. Y. T. Ding, and Z. P. Xu, BionanoSci. **1**, 173 (2011).
12. V. VanBuren, L. Cassimeris, and D. J. Odde, Biophys. J. **89**, 2911 (2005).
13. L. Mahadevan, and T. J. Mitchison, Nature **435**, 895 (2005).
14. Z. Wu, H. W. Wang, and W. Mu, et al, PLoS One **4**, e7291 (2009).
15. M. Huisman, P. G. Bolhuis, and A. Fasolino, Phys. Rev. Lett. **100**, 188301 (2008).
16. X. Y. Ji, and X. Q. Feng, Phys. Rev. E. **84**, 031933 (2011).
17. E. Nogales, and H. W. Wang, Curr. Opin. Cell Biol. **18**, 179 (2006).
18. E. Nogales, and H. W. Wang, Curr. Opin. Struct. Biol. **16**, 221 (2006).
19. F. Gittes, B. Mickey, and J. Nettleton, et al, J. Cell Biol. **4**, 923 (1993).
20. B. Mickey, and J. Howard, J. Cell Biol. **4**, 909 (1995).
21. H. Felgner, R. Frank, and M. Schliwa, J. Cell Sci. **109**, 509 (1996).
22. J. A. Tolomeo, and M. C. Holley, Biophys. J. **73**, 2241 (1997).
23. A. Kis, S. Kasas, and B. Babic, et al, Phys. Rev. Lett. **24**, 248101 (2002).
24. P. J. de Pablo, I. A.T. Schaap, and F. C. MacKintosh, et al, Phys. Rev. Lett. **9**, 098101 (2003).
25. J. A. Tuszynski, T. Luchko, and S. Portet, et al, Eur. Phys. J. E **17**, 29 (2005).
26. A. S. Zeiger, and B. E. Layton, Biophys. J. **95**, 3606 (2008).
27. D. Sept, and F. C. MacKintosh, Phys. Rev. Lett. **104**, 018101 (2010).
28. M. A. Deriu, M. Soncini, and M. Orsi, et al, Biophys. J. **99**, 2190 (2010).
29. V. VanBuren, D. J. Odde, and L. Cassimeris, Proc. Natl. Acad. Sci. U. S. A. **9**, 6035 (2002).
30. M. P. Allen, and D. J . Tildesley, *Computer Simulation of Liquids* (Oxford University Press, Oxford, 1994).
31. L. Mahadevan, A. Vaziri, and M. Das, Europhys. Lett. **77**, 40003 (2007).